Article

Numerical Simulation of Penetration Process of Depleted Uranium Alloy Based on an FEM-SPH Coupling Algorithm

Hui Su [1], Chi Zhang [1], Zhifei Yan [2], Ping Gao [2], Hong Guo [3], Guanchen Pan [4] and Junsheng Wang [1,5,*]

1   School of Materials Science and Engineering, Beijing Institute of Technology, Beijing 100081, China
2   No. 52 Research Institute, China North Industries Group, Baotou 014030, China
3   Metallurgical Research Institute, CNNC North Nuclear Fuel Element Co., Ltd., Baotou 014035, China
4   School of Mechanical Engineering, Beijing Institute of Technology, Beijing 100081, China
5   Advanced Research Institute of Multidisciplinary Science, Beijing Institute of Technology,
     Beijing 100081, China
*   Correspondence: junsheng.wang@bit.edu.cn; Tel.: +86-010-68915043

Abstract: In order to quantitatively study the penetration capability of depleted uranium alloy, a simulation model of bullet impact on target plate with FEM-SPH coupling algorithm was established by using LS-DYNA software, which was combined with Johnson-Cook intrinsic model, Johnson-Cook fracture criterion, and equation of state to conduct a simulation study of alloy bullets made of depleted uranium alloy, tungsten alloy, and high-strength steel to penetrate target plate at 1400 m/s initial velocity. The results show that under the same conditions of initial kinetic energy, initial velocity, and initial volume, the residual kinetic energy of the depleted uranium alloy bullet is 1.14 times that of tungsten alloy and 1.20 times that of high-strength steel, and the residual velocity is 1.14 times that of tungsten alloy and 1.18 times that of steel, and the residual volume is 1.13 times that of tungsten alloy and 1.23 times that of steel after the penetration is completed. The shape of the bullet after penetrating the target plate is relatively sharp, and the diameter of the target hole formed is about 1.70 times the diameter of the projectile, which is significantly larger than 1.54 times that of tungsten alloy and 1.39 times that of high-strength steel, indicating the excellent penetration performance of depleted uranium alloy.

Keywords: FEM-SPH coupling; depleted uranium alloy; penetration performance; numerical simulation

1. Introduction

   With the rapid development of material technology and the continuous optimization of protective materials, the inherent density and strength properties of ordinary steel [1] are difficult to meet the requirements of high intrusion performance. Depleted uranium (DU) alloys [2,3] and tungsten alloys [4,5] have excellent properties such as high density, high hardness, high strength, and good quasi-static mechanical properties, and are commonly used to manufacture the cores of kinetic energy armor-piercing ammunition. In particular, the self-sharpening effect of DU alloys gives them excellent armor-piercing properties, which are of great importance for the manufacture of modern weapons with high destructive and lethal power.

   In recent years, many scholars have conducted extensive comparative studies on the intrusion properties of tungsten alloys and high-strength steels. Giovanni et al. [6] investigated the impact deformation and fracture behavior of armor-piercing projectiles fabricated with three different tool steel cores. Kolmakov et al. [7] discussed the properties of materials used for small arms cores, and the results showed that as a material for special-purpose armor-piercing cores, low-alloy, high-speed steel with high bending strength could be used instead of tungsten alloy. Pranay et al. [8] studied the impact effects of differently shaped projectiles based on ANSYS display dynamics, and the results showed that the

tungsten alloy material of the ovoid warhead was more effective in withstanding velocity impacts than 4340 steel.

Depleted uranium alloys with the same high penetration performance as tungsten alloys have also received much attention from scholars. Wu et al. [9] studied the penetration performance of different shapes of tungsten breakers and uranium breakers by AUTODYN software. The results showed that the penetration capability of uranium breakers was stronger than that of tungsten breakers for the same shape and initial velocity, and the best penetration capability was achieved for cubic breakers. Shi et al. [10] studied the dynamic deformation and damage behavior of uranium-niobium alloys at different artificial aging temperatures by SHPB experiments and analyzed the forming mechanism of the adiabatic shear bond of uranium-niobium alloys under impact loading. Zhu et al. [11] analyzed the velocity characteristics and penetration process of the steel target plates penetrated by DU and tungsten alloy fragments by using finite element software ANSYS/LS-DYNA and the Lagrange algorithm. However, depleted uranium alloys are highly radioactive and have poor storage properties [12], and comparative studies of their intrusion properties with commonly used core materials, tungsten alloys, and high-strength steels have been less reported.

In addition, the action time of the high-speed impact process is generally in the order of microseconds. The stress-strain situation, failure, and damage law of the material during the penetration process are difficult to obtain accurately by experimental methods. Meanwhile, little data information can be obtained due to the long and costly time period of the penetration test. Therefore, to quantitatively analyze the high penetration capability of depleted uranium alloy, LS-DYNA software was used to establish a numerical simulation model of the FEM-SPH coupling algorithm to carry out a numerical simulation of bullet penetration into the target plate. The residual kinetic energy, residual velocity, residual volume, and the hole size after the bullet of depleted uranium alloy, tungsten alloy, and high-strength steel penetration target plate were compared. By analyzing the effective plastic strain of the bullet unit during penetration, the equivalent force distribution of the target plate, and the shape of the bullet after penetration, the reasons for the sharpness of a depleted uranium alloy bullet after failure and dislodgement are investigated. The calculation results in this paper can provide the basis for numerical simulation to gradually improve the penetration capability of armor-piercing ammunition.

2. Materials and Methods

2.1. Material Constitutive Model

The selection and setting of the intrinsic relationship are vital in determining the accuracy of the simulation results when the numerical simulation is used to study the bullet penetration into the target plate. The bullet penetration of the target plate takes place at high strain rates and temperatures, so the effects of strain rate and temperature on material properties need to be considered. The Johnson-Cook [12,13] model provided by LS-DYNA (R11.0.0, Livermore Software Technology Corporation, Livermore, CA, USA) reflects the change in material properties at high strain rates and temperatures and predicts the target plate's yielding and fracture behavior. The yield function is mathematically described as follows [14,15]:

$$\sigma_y = \left(A + \bar{B}\varepsilon^{p^n} \right)\left(1 + Cln\dot{\varepsilon}^* \right)\left(1 - T^{*m} \right) \tag{1}$$

where A is the yield stress, B is the strain hardening constant, C is the strain rate constant, n is the hardening index, m is the thermal softening index, A, B, C, n, and m are the input constants, σ_y is the equivalent force, $\dot{\varepsilon}^*$ is the dimensionless equivalent plastic strain rate, $T^* = (T - T_r)/(T_m - T_r)$ is the dimensionless temperature, T, T_r, and T_m are the current

temperature of the material, the room temperature, and the melting point temperature of the material, respectively. The $\bar{\varepsilon}^p$ is the equivalent plastic strain, which can be described as:

$$\dot{\varepsilon}^* = \frac{\bar{\varepsilon}_e^p}{\dot{\varepsilon}_0}, T^* = \frac{T - T_{room}}{T_{melt} - T_{room}} \tag{2}$$

where T_{room} is the room temperature, and T_{melt} is the melting temperature of the material, $\dot{\varepsilon}^*$ is the dimensionless strain rate, $\dot{\varepsilon}_0$ is the reference strain rate.

The failure criterion for the Johnson-Cook material model uses a maximum failure plastic strain and a maximum hydrostatic pressure criterion, which is mathematically described as:

$$\varepsilon^f = \max([D_1 + D_2 exp D_3 \sigma^*]\left[1 + D_4 ln\dot{\varepsilon}^*\right][1 + D_5 T^*]) \tag{3}$$

where ε^f is the failure, $\sigma^* = p/\sigma_{eff}$, p is the pressure, σ_{eff} is the effective stress, and D_1–D_5 is the material failure parameter. The material fracture damage occurs when the cumulative damage factor D reaches 1.

$$D = \sum \frac{\Lambda \bar{\varepsilon}^p}{\varepsilon^f} \tag{4}$$

2.2. FEM-SPH Coupled Simulation Model

The LS-DYNA nonlinear explicit dynamics software is used for the 3D numerical simulation of the bullet impacting the target plate at high speed. Among them, depleted uranium alloy, tungsten alloy, and high-strength alloy steel (Weldox 900E) are selected as the bullet material. The bullet caliber is Φ8 mm $\times$ 15 mm, and the bullet's initial velocity is 1400 m/s. The material of the target plate is a high-strength alloy steel (AISI-4340), and the target plate is a square plate of 30 mm $\times$ 30 mm $\times$ 5 mm.

Using the FEM-SPH coupling algorithm, the impact area of 3 times the bullet aperture (24 mm) is discretized into SPH mass particles centered at the bullet impact, and the flowing particles are used to describe the large deformation, fragmentation, and flyaway of the target plate. The peripheral part of the target plate is a small deformation area, which is divided into finite cell mesh, and the mesh density is coarsened appropriately to reduce the analysis time. In order to analyze the penetration effect of the bullet, the cell size of the bullet is refined to 0.25 mm $\times$ 0.25 mm, and the JC intrinsic model is used for both the bullet and the target plate. The solid contact mode is used between the SPH particle and the adjacent mesh surface, and the erosion contact is specified between the bullet and the target plate.

In order to save computing time and reduce the computational cost, the quarter simulation calculation model is used in this paper, and the accuracy of the model calculation is ensured by imposing symmetric boundary conditions. The FEM-SPH coupling simulation calculation model is shown in Figure 1. The JC intrinsic model parameters for depleted uranium alloy [16], tungsten alloy [17], Weldox 900E steel [18], and 4340 steel [19] are literature test values, as shown in Table 1.
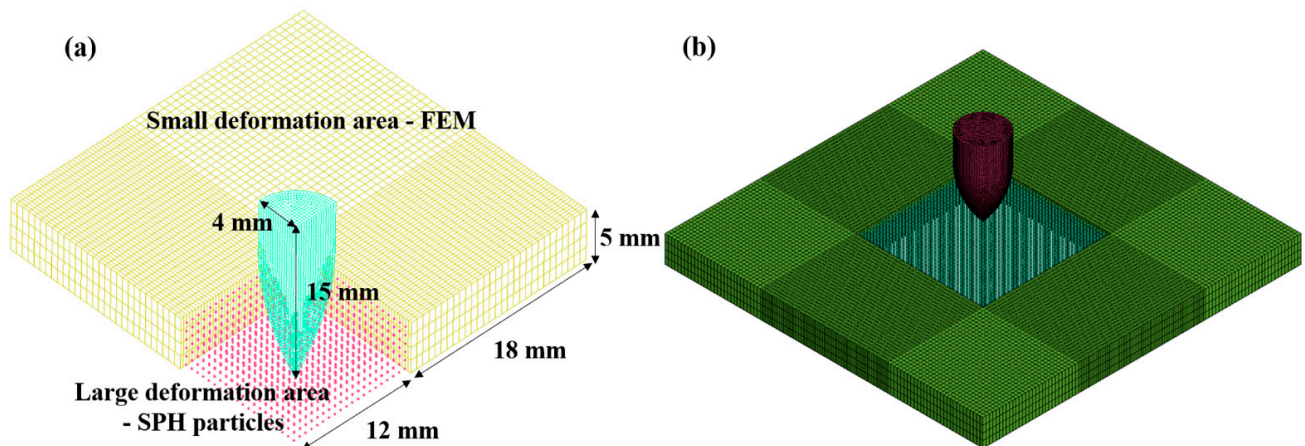
Figure 1. FEM-SPH coupling simulation model between bullet and target. (**a**) quarter model; (**b**) whole model.

Table 1. Material parameters of constitutive models of different alloys.

Materials	Density (g/cm³)	Elastic Modulus (GPa)	Poisson's Ratio	Yield Strength A (MPa)	Strain Hardening Constant B (MPa)	Hardening Index n
DU	18.6	274	0.13	1079	1120	0.250
Tungsten	17.5	360	0.22	1275	624	0.120
900E Steel	7.85	210	0.33	992	364	0.568
4340 Steel	7.83	207	0.29	792	510	0.260

Materials	Strain Rate Constant C	Heat Softening Index m	Melting Temperature (K)	Reference Strain Rate	Specific Heat Capacity (J/Kg·K)
DU	0.0007	1.000	1473	1	117
Tungsten	0.0160	1.030	1723	1	47.7
900E Steel	0.0087	1.131	1800	1	452
4340 Steel	0.0140	1.060	1793	1	477

3. Results

The bullet penetrates the target plate with an initial velocity of 1400 m/s. The numerical simulation of the penetration process of different alloy bullets is shown in Figure 2. At *t* = 2.5 μs, a high-speed collision occurs when the bullet penetrates the target plate. Under high-speed collision, the target plate generates extremely high temperature and pressure, which causes the surface to be depressed. The equivalent force of the contact between the tungsten alloy and the surface of the target plate is significantly larger than that of the depleted uranium alloy and high-strength steel. At *t* = 6 μs, with the bullet intrusion, the bullet head is continuously extruded and ground by the broken target plate material, and the bullet length gradually decreases. The bullet's larger impact force spreads around the target plate, and the intrusion depth of DU alloy is significantly greater than that of tungsten alloy and high-strength steel. At *t* = 9 μs, the target plate material on both sides and within the forward head of the projectile is spalled off by the impact compression and shearing action of the projectile and then reverse splashed and accumulated in the crater. The impact of the depleted uranium alloy on the target plate is enhanced and continues to maintain a large penetration depth. At *t* = 16.5 μs, ablation occurs at the bullet head after the bullet penetrates the target plate. The target plate material piled up on the bullet head loses its restraint and starts to fall off from the top of the bullet. The depleted uranium alloy has a large penetration depth for the same penetration time, demonstrating good penetration performance.
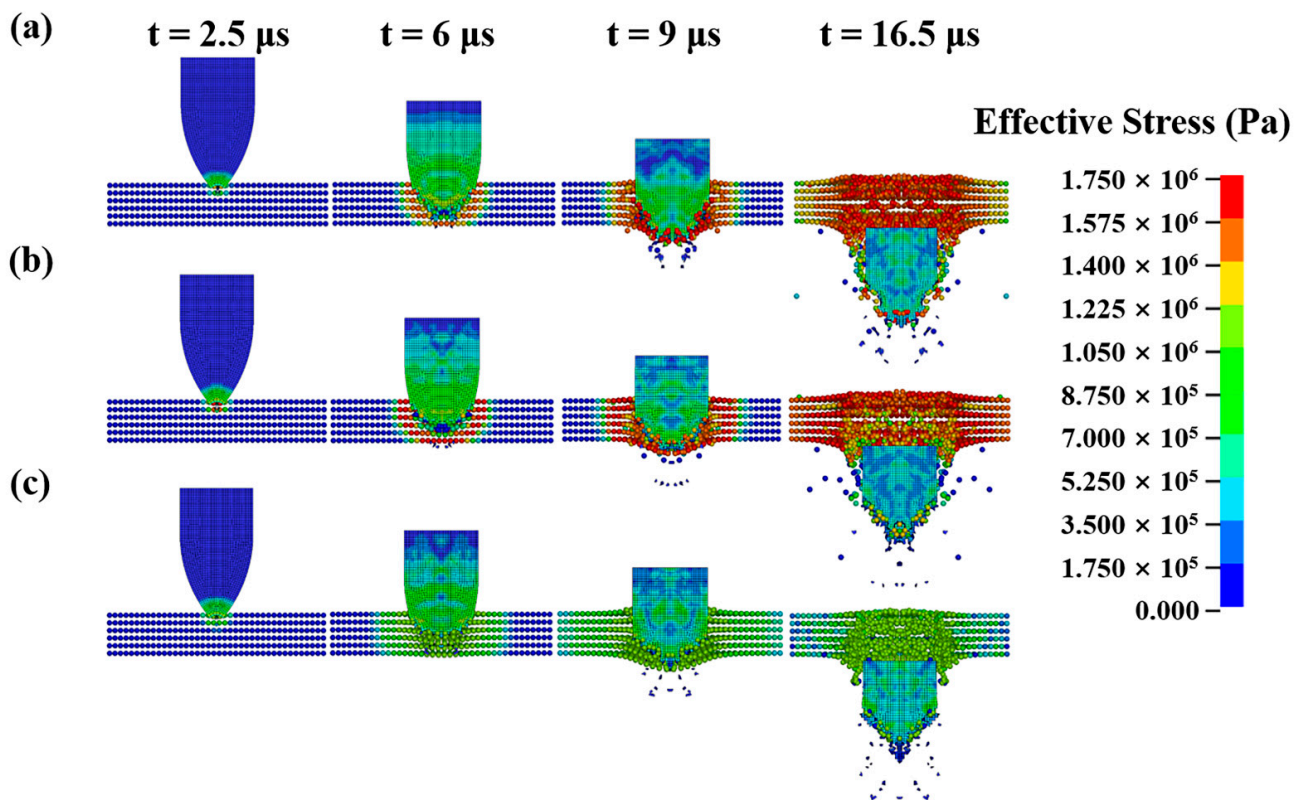
Figure 2. Equivalent stress diagram of bullet penetration process of different alloys (**a**) depleted uranium alloy; (**b**) tungsten alloy; (**c**) high strength steel.

Figure 3 shows the variation of bullet kinetic energy and velocity with penetration time during bullet of different materials alloy penetration target plate. Before the intrusion occurs at t = 2.5 μs, the kinetic energy and initial velocity of the bullet are 1018.32 KJ and 1400 m/s, respectively. As the intrusion time increases, the bullet starts to collide with the target plate, and the kinetic energy and velocity of the bullet decrease significantly at t = 6 μs. At t = 15 μs, the kinetic energy and velocity of the bullet tend to level off, which marks the end of the intrusion process. According to the conservation of energy, the energy lost by the bullet in the process of penetration has roughly three destinations: bullet fragmentation and splash, plastic deformation of the target plate, and energy consumption of the target plate fragmentation. The direction of bullet fragmentation and splash is generally opposite to the direction of impact. This jet does not have the ability to destroy the target plate but loses much kinetic energy from the bullet. After the end of the intrusion, the residual kinetic energy and velocity of DU alloy are 640.5 KJ and 978.3 m/s, respectively. The residual kinetic energy and velocity of tungsten alloy are 559.5 KJ and 860.9 m/s, respectively. The residual kinetic energy and velocity of high-strength steel are 533.8 KJ and 828.1 m/s, respectively. At the end of the intrusion, the kinetic energy and velocity consumption of DU alloy was 37% and 30%, respectively. Which was significantly lower than that of tungsten alloy 45% and 39%, and high-strength steel 48% and 41%, respectively. This indicates that DU alloy still had good intrusion performance at the end of the intrusion.
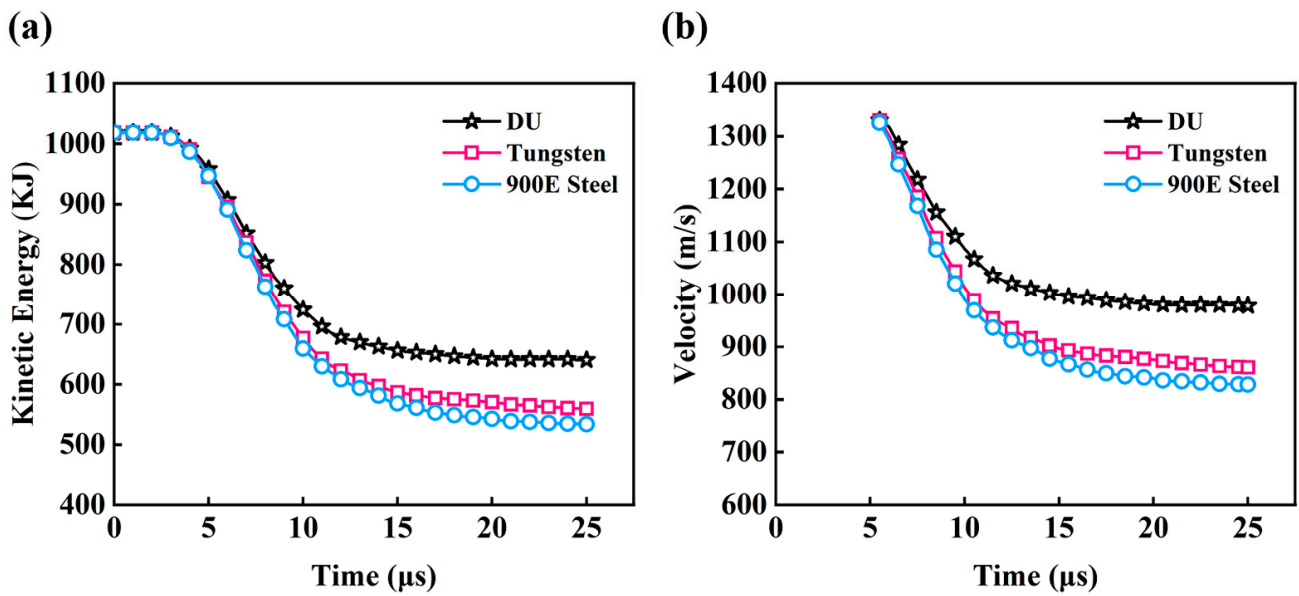
(a)

(b)

Figure 3. Variation of kinetic energy and velocity of different alloy bullets with penetration time (**a**) kinetic energy–time; (**b**) velocity–time.

The bullet unit is dislodged by reaching the failure criterion during penetration, and its volume varies with the penetration time, as shown in Figure 4. After the bullet penetrates the target plate, it collides with the target plate at high speed. The bullet head is continuously squeezed and ground by the broken target plate material, and the volume decreases continuously, as shown in Figure 4. After the end of the intrusion, the volume of DU alloy, tungsten alloy, and high-strength steel was reduced from 131.5 to 95.1, 84.2, and 77.4, respectively.
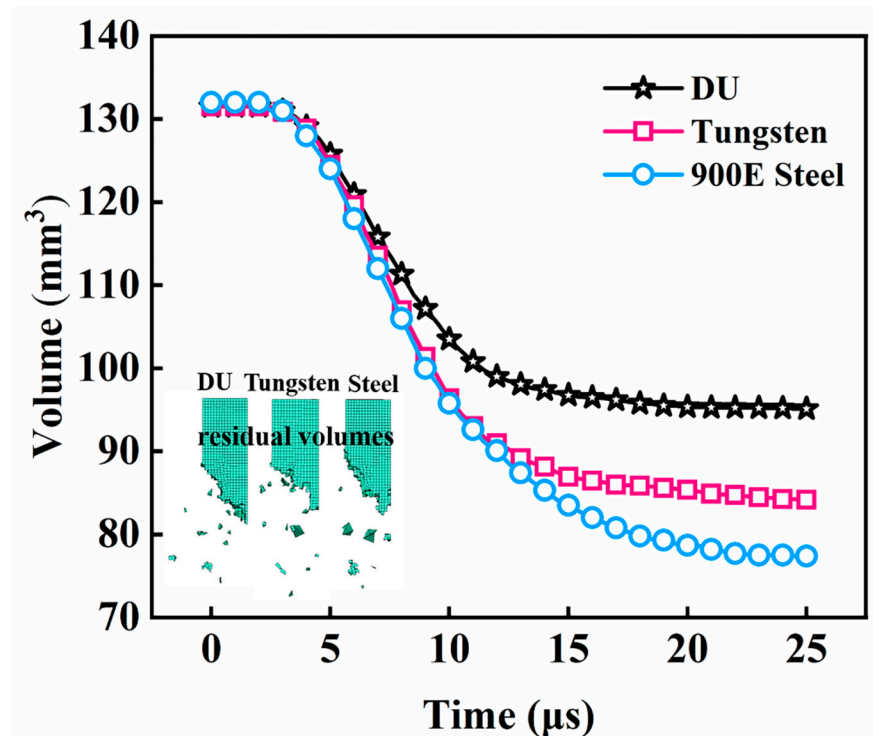

Figure 4. Variation of bullet volume with penetration time during penetration of different alloys.

The displacement variation of surface nodes 1−7 along the impact direction after the intrusion of different alloy materials into the target plate material is presented in Figure 5. After the bullet penetrates the target plate, the target plate surface material fails and peels off with the impact of the bullet. The deformation of node 1 near the center of the penetration is the largest, and the deformation of node 7 far from the penetration area is the smallest. The nodal displacement curve roughly reflects the shape of the target plate after the damage. The shape of the bullet reflects the penetration ability of the bullet during penetration, as shown in Figure 5b. It can be seen, Depleted uranium bullets have sharper heads than tungsten and high-tensile steel bullets, maintaining good penetration properties. Whereas tungsten bullets and high-tensile steel bullets form "mushroom heads", so the piercing capability is relatively lower. The deformation diagram of the head tips of depleted uranium alloy and tungsten alloy bullets [17] is shown in Figure 5c. It can be seen that this is in good agreement with the bullet shape after penetration (Figure 5b). This indicates that the depleted uranium alloy has excellent penetration properties both during and after the penetration process and also verifies the accuracy of the simulation results in this paper.
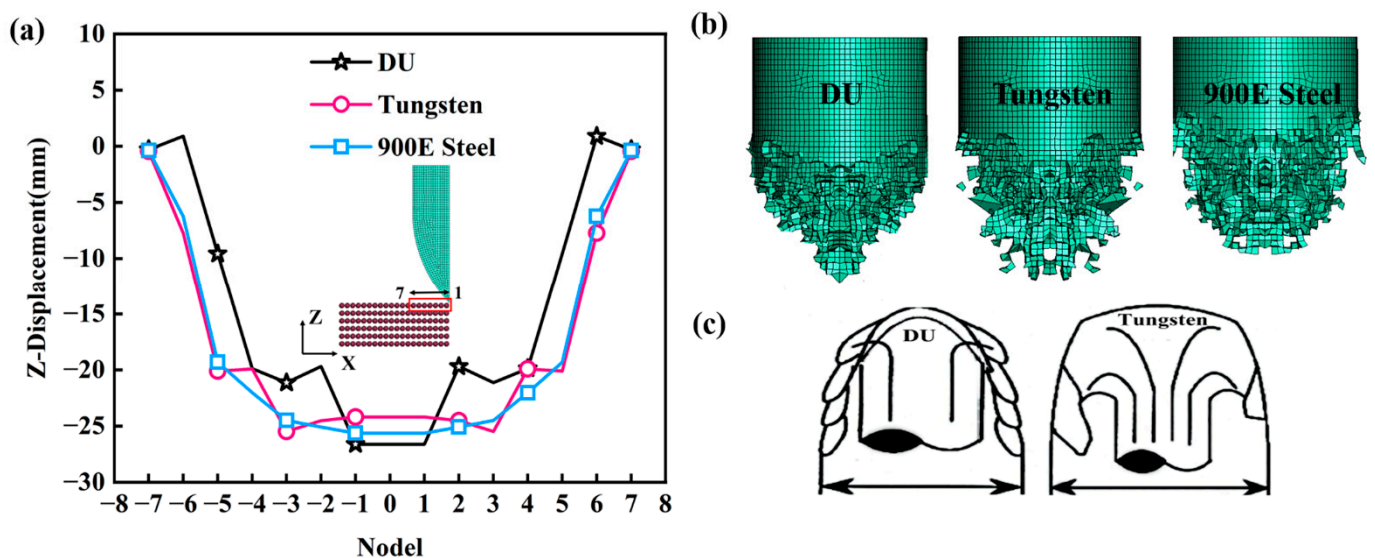

Figure 5. Displacement changes of surface nodes along the impact direction during penetration of different alloys. (**a**) Node displacement distance; (**b**) Comparison of the shape of the bullet after penetration; (**c**) Tip deformation of depleted uranium and tungsten alloy amour piercing warheads [20].

The front view of the target hole formed by different alloy materials after penetrating the target plate is demonstrated in Figure 6. When the bullet hits the target plate at high speed, the ballistic channel is flat at the initial stage of penetration. The material on the back of the target plate is in a stretched state as the intrusion time increases. The ballistic channel gradually becomes larger and forms a target hole. By measurement, the diameter of the target holes formed by DU alloy, tungsten alloy, and high-strength steel after penetrating the target plate is about 13.6 mm, 12.3 mm, and 11.1 mm, respectively. The target holes formed by DU and tungsten alloy are more regular than that of high-strength steel and become oval.
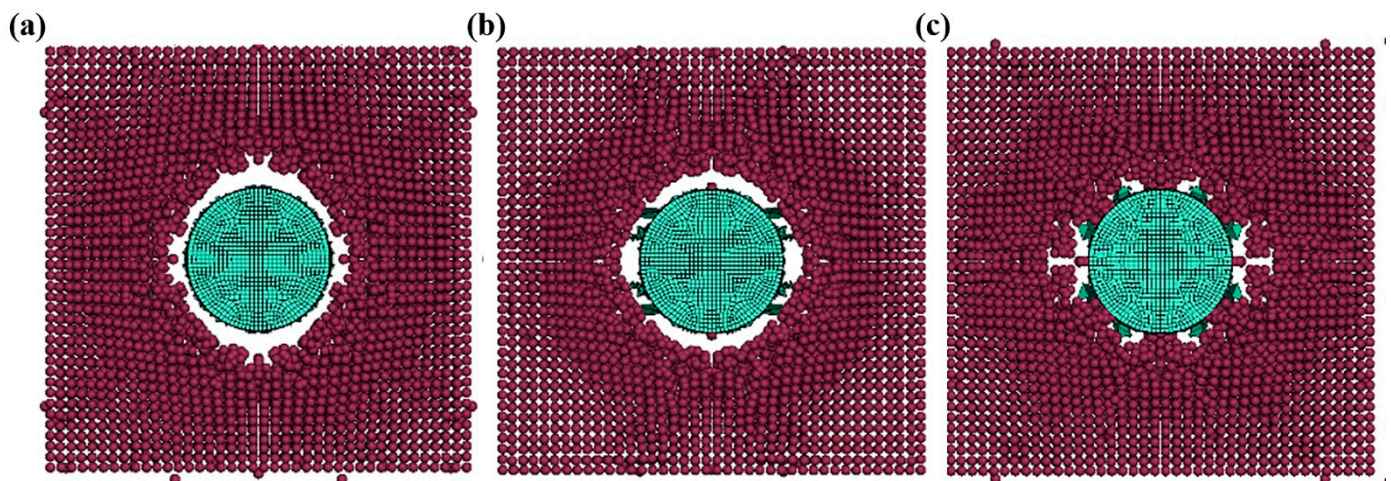
Figure 6. Front view of target hole formed after different alloy materials penetrate the target plate. (**a**) Du alloy; (**b**) tungsten alloy; (**c**) high-strength steel.

To further understand the exfoliation ability of DU alloy material during the intrusion process, the effective plastic strain curves of the typical cell A–F on the bullet material were extracted during the intrusion process, as shown in Figure 7. It can be seen that as the intrusion time increases, the order of strain failure that occurs in the cell is A < C < B < E < D < F. The center unit E of the projectile is slower to fail than the outer units D and F. The center units A and C are slower to fail than the outer units B, D, and E. This indicates that during the process of bullet penetration, the outer material of the bullet body fails and flakes off due to plastic strain first, and the center of the bullet body fails more slowly, which makes the bullet head sharper and can continue to maintain the good penetration ability of the bullet body.
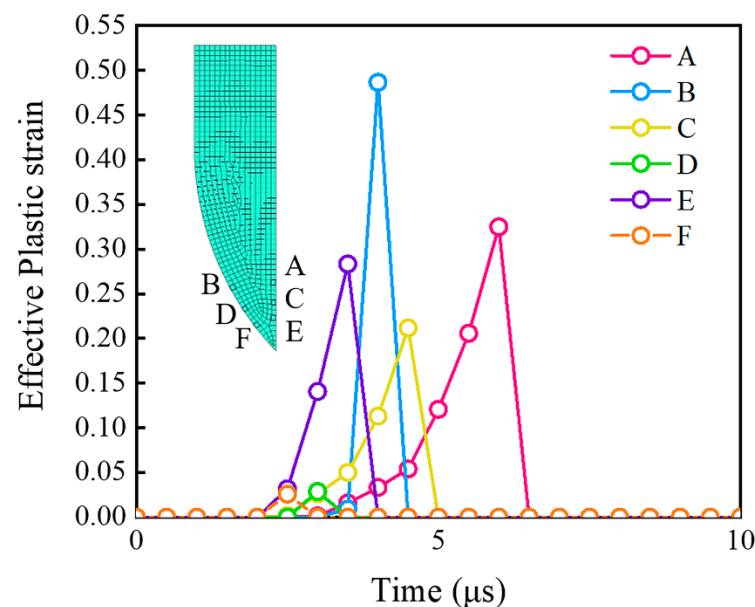

Figure 7. Effective plastic strain curves of typical elements during DU bullet penetration.

The variation of the reaction force on the contact surface of the target plate with the depth of penetration is shown in Figure 8a. The distribution of the equivalent stress at the maximum reaction force is presented in Figure 8b. As seen in Figure 8a, the target plate cross-sectional reaction force increases with the bullet penetration depth. After reaching the maximum reaction force (22.3 KN), that is, the critical point of bullet penetration of the

target plate, the target plate cross-sectional reaction force begins to decrease, and at this time, the maximum equivalent force of the target plate is 1661 MPa, as shown in Figure 8b.
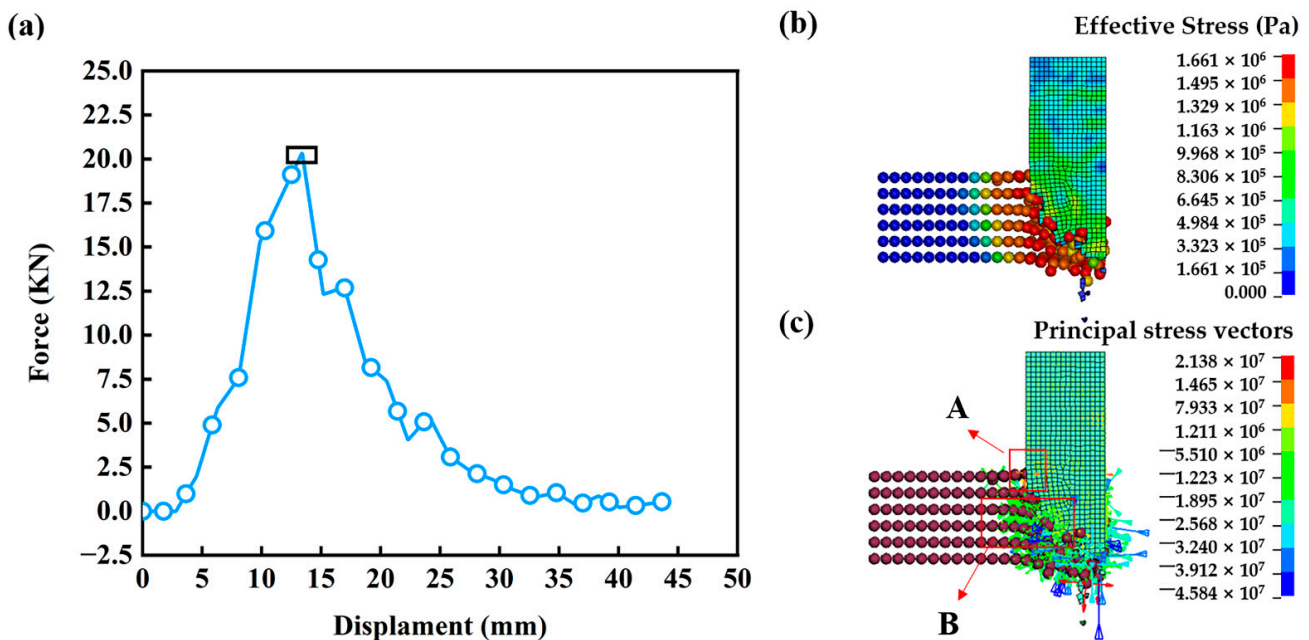

Figure 8. (**a**) The variation of reaction force on the contact surface of the target plate with the depth of the invasion side, (**b**) the equivalent stress distribution diagram, and (**c**) the main stress vectors at the maximum reaction force.

During penetration, the target plate is subjected to forces from different directions of the bullet, and the Main stress vectors at the maximum reaction force are illustrated in Figure 8c, where region A is the target plate open area, and region B is the plastic expansion area. The color of the vector arrow shows the stress state, and the direction of the arrow indicates the magnitude of the stress. As seen, the stress vector of area A is orange, and the vector arrow is perpendicular to the cross-section of the target plate pointing to the outside. It indicates that the open area of the target plate is subjected to a circular tensile stress perpendicular to the cross-section of the target plate. Under the action of tensile stresses, the target plate undergoes cumulative damage and breaks down after reaching the failure judgment criteria. The stress vector of area B is blue and green, and the vector arrow is perpendicular to the cross-section of the target plate pointing to the inside. It indicates that the plastic expansion zone of the target plate is subjected to the circumferential compressive stress perpendicular to the cross-section of the target plate. Through observation, it can be seen that the plastic deformation in area B is serious, and the plastic deformation of the target plate material keeps increasing under the continuous action of the compressive stress of the projectile, which reaches the judgment standard of strain failure and fails, and finally falls off after the projectile penetrates the target plate.

To quantitatively analyze the high penetration performance of depleted uranium alloys, Table 2 summarizes the parameters related to the kinetic energy, velocity, and volume of the bullet and the size of the target hole diameter for different alloy materials. After penetrating into the target plate, the bullet collides with the target plate at high speed, and its kinetic energy, velocity, and volume decrease continuously. After penetration, DU alloy loses 37% kinetic energy, loses 30% velocity, and reduces 28% volume, tungsten alloy loses 45% kinetic energy, loses 39% velocity, and loses 36% volume, and high-strength steel loses 48% kinetic energy, loses 41% velocity and reduces 41% volume. The comparison shows that the penetration performance of DU alloy is significantly better than that of tungsten alloy and high-strength steel.

Table 2. Relevant parameters of bullets made of different alloy materials.

Materials	Initial Kinetic Energy (KJ)	Residual Kinetic Energy (KJ)	Kinetic Energy Consumption	Initial Speed (m/s)	Residual Speed (m/s)	Speed Loss
DU	1018.32	640.5	37%	1400	978.3	30%
Tungsten	1018.32	559.5	45%	1400	860.9	39%
900E Steel	1018.32	533.8	48%	1400	828.1	41%

Materials	Initial Volume (mm^3)	Residual Volume (mm^3)	Volume Loss	Bullet Diameter A (mm)	Target Hole Diameter B (mm)	B/A
DU	132	95.1	28%	8	13.6	1.70
Tungsten	132	84.2	36%	8	12.3	1.54
900E Steel	132	77.4	41%	8	11.1	1.39

The experimental and simulation results of depleted uranium alloy, tungsten alloy, and high-strength steel intruding through target plates of different materials are summarized in Table 3. It can be seen that the results of this paper maintain a good agreement with the overall trend of the literature results, which verifies the accuracy of the simulation results of this paper.

Table 3. Related parameters of penetration process of different alloys.

Bullet Material	Target Plate Material	Thickness of Target Plate (mm)	Initial Speed (m/s)	Remaining Speed (m/s)	Ref.
DU	4340 Steel	5	1400	978.9	This work
Tungsten	4340 Steel	5	1400	860.9	This work
900E Steel	4340 Steel	5	1400	828.1	This work
DU	Q235	10	1300	555	[9]
Tungsten	Q235	10	1300	509.3	[9]
Tungsten	Armored steel	50	1609	733	[4]
4340 Steel	Al7075	12.5	1500	1460.22	[8]
Tungsten	Al7075	12.5	1500	1481.73	[8]
4340 Steel	Al7075	18	1400	1341.16	[8]
Tungsten	Al7075	18	1400	1372.91	[8]

4. Conclusions

In this paper, the penetration capability of depleted uranium alloy, tungsten alloy, and high-strength steel is studied quantitatively and comparatively through the numerical simulation model of the FEM-SPH coupling algorithm. Conclusions are drawn as follows.

(1) Under the condition of the same variables, the penetration performance of DU alloy bullets is significantly higher than that of tungsten and high-strength steel. The sharper shape of the bullet after penetration by DU alloy improves the penetration capability of the alloy. The tungsten alloy and high tensile steel penetrated bullets with a "mushroom heads" shape and therefore had a relatively low penetration capacity.

(2) In the penetration process, the material of DU alloy is first detached by plastic deformation failure in the area far from the center of the bullet, and the material in the center of the bullet fails more slowly. The shape of the bullet after penetrating the target plate is relatively sharp, thus improving the penetration capability of DU alloy.

(3) The diameter of the target hole formed by the DU alloy after penetrating the target plate is large, about 1.70 times the diameter of the bullet, which is significantly larger than that of tungsten alloy (1.54 times) and high-strength steel (1.39 times), indicating that the DU alloy bullet has a greater killing capacity during penetration.

Quantitative evaluation of the penetration performance of depleted uranium alloys, tungsten alloys, and high-strength steels can provide a basis for numerical simulations to improve the penetration capability of armor-piercing bullets gradually. However, there are many influencing factors in the actual service environment of the bullets. Therefore, obtaining a large amount of experimental data and establishing a database of test and simulation results will be the focus of the following research.

References

1. Liu, X.Y.; Ma, H.H.; Fan, F. Low-velocity impact behavior of SWRH82B steel wires considering different section shapes based on experiments and simulations. *J. Constr. Steel Res.* **2023**, *200*, 107660. [CrossRef]
2. Parker, H.M.O.; Beaumont, J.S.; Joyce, M.J. Passive, non-intrusive assay of depleted uranium. *J. Hazard. Mater.* **2019**, *364*, 293–299. [CrossRef] [PubMed]
3. Guo, Y.K.; Shuai, M.B.; Zou, D.L.; Zhao, Y.W.; Xiao, D.W. Formation and Evolution Mechanism of Adiabatic Shear Bands in U-5.7Nb Alloy Subjected to Dynamic Loading. *Rare Met. Mater. Eng.* **2018**, *47*, 1459–1465.
4. Senthil, P.P.; Reddy, P.R.S.; Reddy, T.S.; Kumar, K.S.; Madhu, V. Scaled wha long rod projectile impact against an armour steel. *Hum. Factors Mech. Eng. Def. Saf.* **2019**, *3*, 1–8. [CrossRef]
5. Zhou, F.; Du, C.X.; Du, Z.H.; Gao, G.F.; Cheng, C.; Wang, X.D. Penetration Gain Study of a Tungsten-Fiber/Zr-Based Metallic Glass Matrix Composite. *Crystal* **2022**, *12*, 284. [CrossRef]
6. Benedetto, G.D.; Matteis, P.; Scavino, G. Impact behavior and ballistic efficiency of armor-piercing projectiles with tool steel cores. *Int. J. Impact Eng.* **2018**, *115*, 10–18. [CrossRef]
7. Kolmakov, A.G.; Bannykh, I.O.; Antipov, V.I.; Vinogradov, L.V.; Sevost'yanov, M.A. Materials for Bullet Cores. *Russ. Metall.* **2021**, *2021*, 351–362. [CrossRef]
8. Pranay, V.; Panigrahi, S. Effects of spinning on residual velocity of ogive-nosed projectile undergoing ordnance velocity impact. *Proceedings of the Institution of Mechanical Engineers, Part C: Journal of Mechanical Engineering Science.* **2022**, *236*, 1685–1697. [CrossRef]
9. Wu, F.D.; Zhao, H.D. Study on the Penetration Performance of Different Shaped DU Alloy. *Chin. J. High Press. Phys.* **2018**, *32*, 055103.
10. Shi, J.; Wang, X.Y.; Zhao, Y.W. Effect of heat treatment on localization of uranium alloy deformation. *Rare Met. Mater. Eng.* **2014**, *11*, 2836–2840.
11. Zhu, F.L.; Yang, C.; Zhu, G.L. Numerical simulation study on penetration performance of depleted Uranium (DU) alloy fragments. *Def. Technol.* **2021**, *17*, 50–55. [CrossRef]
12. Shen, X.H.; Zhang, D.H.; Yao, C.F.; Tan, L.; Li, X.Y. Research on parameter identification of Johnson–Cook constitutive model for TC17 titanium alloy cutting simulation. *Mater. Commun.* **2022**, *31*, 103772. [CrossRef]
13. Vasu, K.R.S.; Vinith, Y.G.; Uday, S.G.; Suneesh, G.; Krishna, M.B. A review on Johnson Cook material model. *Mater. Proc.* **2022**, *62*, 3450–3456.
14. Hallquist, J. LS-DYNA Keyword User's Manual, Version: R 13.0. 2021. Available online: https://www.dynasupport.com/manuals/ls-dyna-manuals/ls-dyna_manual_volume_i_r13.pdf/view (accessed on 6 May 2022).
15. Johnson, G.R.; Cook, W.H. Fracture characteristics of three metals subjected to various strains, strain rates, temperatures and pressures. *Eng. Fract. Mech.* **1985**, *21*, 31–48. [CrossRef]
16. James, D.W.; Scott, A.M.; Carl, E.W.; Paul, O.L. Penetration of boron carbide, aluminum, and beryllium alloys by depleted ura-nium rods: Modeling and experimentation. *Int. J. Impact Eng.* **2006**, *33*, 826–836.
17. Herve, C.; Guy, N.; Claude, A. Relation between shear banding and penetration characteristics of conventional tungsten alloys. *Int. J. Impact Eng.* **2007**, *34*, 412–423.
18. Dey, S.; Børvik, T.; Hopperstad, O.S. The effect of target strength on the perforation of steel plates using three different projectile nose shapes. *Int. J. Impact Eng.* **2004**, *30*, 1005–1038. [CrossRef]

19. Balbaa, M.; Nasr, M.N.A.; Elgamal, H.A. Sensitivity analysis on the effect of laser power on residual stresses when laser-assisted machining AISI 4340. *Procedia CIRP* **2017**, *58*, 31–36. [CrossRef]

20. Magness, L.S.; Farrand, T.G. Deformation behaviour and its relationship to the penetration performance of high-density KE penetrator materials. In Proceedings of the 1990 Army Science Conference, Durham, NC, USA, 12–15 June 1990; pp. 149–164.